PLANETARY SCIENCE

Enrichment of moderately volatile elements in first-generation planetesimals of the inner Solar System

Damanveer S. Grewal[1,2]*, Surjyendu Bhattacharjee[3], Bidong Zhang[4], Nicole X. Nie[5], Yoshinori Miyazaki[3]

The depletion of moderately volatile elements (MVEs) in terrestrial planets remains poorly understood, with explanations including partial nebular condensation and MVE loss during planetesimal differentiation or collisions. In this study, we use magmatic iron meteorites to reconstruct the MVE inventory of the earliest inner [noncarbonaceous (NC)] and outer [carbonaceous (CC)] Solar System planetesimals. We show that several NC and CC iron meteorite parent bodies (IMPBs) exhibit chondrite-like MVE abundances, indicating that "first-generation" inner Solar System planetesimals were remarkably MVE rich. Consistent with isotopic signatures of MVEs in Earth and Mars, these planetesimals made a substantial contribution to the MVE inventories of terrestrial planets. Variations in MVE abundances among IMPBs, particularly the two volatile-depleted NC and CC IMPBs (IVA and IVB), reflect secondary volatile loss after disruption of their parent bodies. Consequently, MVE depletion in terrestrial planets is more closely linked to the protracted history of MVE loss during planetesimal collisions rather than incomplete condensation or MVE loss during planetesimal differentiation.

INTRODUCTION

Tracking the origin of moderately volatile elements [MVEs; 50% condensation temperature (T_C) between main group silicates and troilite (~1450 to 650 K)] in terrestrial planets is key to understanding planet formation in our Solar System and beyond. Earth and Mars are MVE depleted compared to chondrites (*1*–*3*). The primary cause behind their MVE depletion, whether because of incomplete condensation of primordial solids from the nebular gas or volatile loss during either planetesimal differentiation or collisions, is highly debated (*2*, *4*, *5*). Meteorites serve as a reference to trace the MVE inventory in the building blocks of planets. They sample early Solar System planetesimals, potentially preserving chemical signatures of the processes that contribute to the MVE depleted character of terrestrial planets. Isotopic signatures of several elements in meteorites suggest that Earth and Mars predominantly grew through the accretion of inner Solar System [or noncarbonaceous (NC)] planetesimals, with only a small contribution (up to 4 to 5% for Earth and almost negligible for Mars) from the outer Solar System [or carbonaceous (CC)] reservoir (*6*, *7*). Therefore, constraining the chemical compositions of the early-formed NC planetesimals is critical to elucidate the underlying cause of MVE depletion observed in terrestrial planets.

NC meteorites indicate substantial variations in the MVE abundances of inner Solar System planetesimals. Abundances of several MVEs in enstatite, ordinary, and Rumuruti chondrites (ECs, OCs, and RCs, respectively) are within the range of those of CI chondrites (*8*, *9*)—chemically the most primitive materials in the Solar System. Primitive achondrites like brachinites, acapulcoites/lodranites, ureilites, and winonaites also sample planetesimals that likely accreted materials with chondrite-like MVE abundances (*10*, *11*). In contrast, differentiated achondrites like angrites and howardite-eucrite-diogenites (HEDs) are extremely MVE depleted (*12*, *13*). For example, Rb/Sr and K/U ratios of HEDs are ~10 to 100 times lower than those of ECs and OCs, while anomalously alkali-depleted angrites have ratios that are ~100 to 1000 times lower (*2*, *3*, *12*, *13*). Since the building blocks of terrestrial planets formed rapidly [likely within ~1 to 2 million years (Myr) after calcium-aluminum–rich inclusion (CAI) formation] (*14*–*16*), the parent bodies of angrites and HEDs, which accreted earlier than chondrite and primitive achondrite parent bodies (*17*, *18*), are considered more representative of the primary building blocks of terrestrial planets (*5*, *19*). However, there is a lack of consensus whether the MVE depletion observed in angrites and HEDs is a primitive signature or the result of secondary volatile loss after accretion. Some researchers have associated the MVE depletion in these meteorites to incomplete condensation in the nebular environment (*5*, *19*, *20*). This idea aligns with some astrophysical models that propose that the earliest NC planetesimals formed at the silicate condensation line ($T_{midplane}$ > 1300 K) (*14*, *21*). Alternately, MVE depletion in angrites and HEDs has been associated with volatile loss from their parent bodies during large-scale melting events, induced by either ^{26}Al decay or impacts, in volatile-bearing planetesimals (*22*–*24*). Efficient volatile loss during vapor-silicate melt exchange at the surface of planetesimals (e.g., in a convecting magma ocean) implies that the differentiated seeds of terrestrial planets could be MVE depleted even if the parent bodies originally formed from MVE-bearing materials (*2*, *22*, *24*). Consequently, the MVE depletion of terrestrial planets, regardless of the primitive compositions of early NC planetesimals, is widely believed to be a result of the early accretion of almost volatile-free differentiated planetesimals followed by the accretion of volatile-bearing materials toward the later stages of planetary growth (*5*, *25*, *26*).

While angrites and HEDs serve as crucial references for deducing the bulk chemical compositions of the seeds of terrestrial planets, this approach has several critical limitations. These meteorites consist mainly of basaltic rocks that sample crustal to subcrustal layers of their parent bodies (*12*, *13*). Consequently, the depletion of some MVEs, and their associated isotopic fractionation, in angrites

[1]School of Molecular Sciences, Arizona State University, Tempe, AZ 85281, USA. [2]School of Earth and Space Exploration, Arizona State University, Tempe, AZ 85281, USA. [3]Division of Geological and Planetary Sciences, California Institute of Technology, Pasadena, CA 91125, USA. [4]Department of Earth, Environmental and Planetary Sciences, Rice University, Houston, TX 77005, USA. [5]Department of Earth, Atmospheric, and Planetary Sciences, Massachusetts Institute of Technology, Cambridge, MA 02139, USA.
*Corresponding author. Email: damanveer.grewal@asu.edu

and HEDs can also be attributed to near-surface magmatic processes and localized impact melting (*4*, *12*, *13*, *27*). This raises concerns whether the MVE depletion in angrites and HEDs is limited to the loss of MVEs solely from the near-surface layers of their parent bodies rather than affecting the entire planetesimals. Alternately, if angrites and HEDs sample "second-generation" planetesimals that accreted from the volatile-depleted ejecta of MVE-bearing "first-generation" planetesimals (*28*–*30*), their utility in deducing the chemical compositions of the earliest-formed NC planetesimals would be severely limited. Furthermore, angrites and HEDs originate from only two parent bodies, which underscores issues about their statistical representativeness compared to NC chondrites and primitive achondrites that sample multiple parent bodies. Therefore, while angrites and HEDs provide valuable insights, these limitations warrant caution when relying solely on them to infer the chemical compositions of the seeds of terrestrial planets during the earliest stages of planet formation. Further consideration of a broader range of meteorites is necessary for a more comprehensive understanding.

In this study, we introduce an alternate approach by using magmatic NC iron meteorites—remnants of the metallic cores of differentiated planetesimals (*31*)—as a proxy to reconstruct the bulk chemical compositions of the earliest-formed planetesimals in the inner Solar System. Metal-silicate equilibration in largely molten planetesimals established the chemical compositions of their parent cores sampled by magmatic irons (*32*–*36*). We have used the elemental abundances in the parent cores of magmatic irons (*37*–*40*), along with their respective liquid metal-liquid silicate partition coefficients, to reconstruct the bulk chemical compositions of the iron meteorite parent bodies (IMPBs). This exercise allows us to constrain the abundances of several siderophile and chalcophile MVEs, encompassing a broad range of volatilities (50% T_C = ~1300 to 600 K), in IMPBs. Using magmatic irons to reconstruct the MVE abundances in the earliest-formed planetesimals offers several notable advantages:

1) In contrast to angrites and HEDs, the chemical compositions of the parent cores of magmatic irons remain unaffected by near-surface magmatic differentiation processes and impacts.

2) Unlike angrites and HEDs, whose chemical compositions were likely influenced by a protracted and complex series of more than one parent body process (*12*, *13*), relatively simple fractional crystallization models can be used to track the compositions of the parent cores of magmatic irons (*33*, *38*, *40*, *41*).

3) The accretion of NC IMPBs commenced within ~0.3 to 1 Myr after CAI formation (*15*, *42*, *43*). Larger uncertainties in the accretion ages of angrite and HED parent bodies (*18*) suggest that NC IMPBs are better representatives of the "first-generation" planetesimals in the inner Solar System.

4) Magmatic irons, in addition to sampling NC planetesimals, also sample the earliest-formed planetesimals in the CC reservoir (*15*, *42*). Comparisons of the reconstructed MVE abundances in NC and CC IMPBs are crucial for investigating how nebular condensation influenced the chemical compositions of primordial materials in the inner and outer parts of the solar protoplanetary disk.

5) Grouped magmatic NC (IC, IIAB, IIIAB, IIIE, and IVA) and CC [IIC, IID, IIF, IIIF, IVB, and South Byron trio (SBT)] irons sample five and six distinct parent bodies from the inner and outer Solar System reservoirs, respectively. This makes NC IMPBs a larger archive of the chemical compositions of the earliest-formed planetesimals compared to angrites and HEDs.

To summarize, NC magmatic irons are potentially an excellent proxy to quantitatively determine the bulk MVE abundances in the earliest-formed planetesimals in the inner Solar System. The results can then be used to constrain MVE abundances of primordial materials within the inner disk and their fate during early stages of planet formation. Understanding these aspects is critical to better elucidate the role of early Solar System processes that define the MVE-depleted character of terrestrial planets.

In this study, we used the abundances of siderophile and chalcophile elements in the parent cores of magmatic irons, along with their respective metal-silicate partition coefficients, to reconstruct the bulk compositions of the NC and CC IMPBs using the following mass balance equation

$$C_i^{\text{bulk}} = \frac{C_i^{\text{core}}\left(r + 1/D_i^{\text{metal/silicate}}\right)}{r+1} \quad (1)$$

where C_i is the concentration of an element i in a reservoir, r is the core/mantle mass ratio of the planetesimal, and $D_i^{\text{metal/silicate}}$ is the partition coefficient of an element between metallic and silicate melt. This mass balance equation has been used to capture elemental distribution during the relatively simple core-mantle differentiation events in planetesimal-sized IMPBs (*32*, *34*–*36*, *44*, *45*). Core/mantle mass ratios (r) for IMPBs have been established previously by determining the enrichment of highly siderophile elements (HSEs) in their parent cores compared to chondrites (*33*). Elemental concentrations in the parent cores of NC and CC irons were previously determined by using elemental abundances in magmatic irons in conjunction with fractional crystallization models (*37*–*40*). To estimate the relevant $D_i^{\text{metal/silicate}}$ for each IMPB, we used parametrized equations from previous studies (*46*–*52*), considering relevant thermodynamic parameters specific to each IMPB, such as oxygen fugacity (fO_2) and alloy melt composition (*33*, *38*, *53*) (see Materials and Methods for details). Given the substantial variations in the siderophile characteristics of elements present in the parent cores of magmatic irons, this exercise is critical to quantitatively constrain the bulk abundances of several siderophile and chalcophile elements, including those of MVEs, in NC and CC IMPBs.

RESULTS

Compared to HSEs ($D_i^{\text{metal/silicate}}$ = ~10^4 to 10^8) like Re, Ir, Ru, Pt, Rh, and Pd, refractory elements like Mo, Ni, Co, and Fe exhibit moderately siderophile characteristics ($D_i^{\text{metal/silicate}}$ = ~1 to 10^3) under conditions relevant for metal-silicate equilibration in NC and CC IMPBs (fig. S1). Almost all MVEs (Au, As, Cu, Ga, Sb, Ge, and S) also exhibit moderately siderophile behavior ($D_i^{\text{metal/silicate}}$ = ~5 to 10^3), except for S, which is lithophile for the more reduced IIAB IMPB, whereas P shows lithophile behavior ($D_i^{\text{metal/silicate}}$ = ~0.1 to 0.8) for all CC IMPBs and most NC IMPBs, except for IIAB and IVA IMPBs.

Analogous to chondrites, the bulk abundances of refractory elements in all NC and CC IMPBs are within a factor of ~1 to 2 × CI (except for IID, which is enriched in Re, Ir, and Ru by a factor of ~3 to 5 × CI) (fig. S2A, Fig. 1A, and table S1). Among MVEs, there is a monotonic depletion with 50% T_C from Au to Cu in NC IMPBs (Fig. 1A and table S1). They have chondritic Au contents (~0.9 to 1.2 × CI), whereas they are depleted in As (~0.5 to 0.8 × CI) and Cu (0.2 to

0.5 × CI). The Cu, Ga, Sb, Ge, and S contents in each NC IMPB (except IVA) are not fractionated and do not exhibit a volatile depletion trend. For example, the abundances of these elements in the IC IMPB are ~0.5 to 1 × CI, whereas their abundances in the IIAB, IIAB, and IIIE IMPBs are ~0.3 to 0.6 × CI, ~0.2 to 0.4 × CI, and ~0.2 to 0.4 × CI, respectively. Sulfur shows an anomalous enrichment (~4 × CI) for the IIAB IMPB. This enrichment could be an artifact of the order of magnitude lower fO_2 for core-mantle differentiation [logfO_2 = IW–3.2; thermodynamic parameter that primarily controls $D_S^{metal/silicate}$ under conditions relevant for planetesimal differentiation (*54*)] estimated for its parent body compared to other NC IMPBs (logfO_2 = IW–2.1 to IW–1.7) (*53*). The fO_2 of core-mantle differentiation in IMPBs is determined from the depletion of Fe/Ni ratio in their parent cores compared to that in chondrites, assuming that the depletion is caused by the retention of oxidized Fe in the mantles (*53*). Should the bulk Fe/Ni ratio of the IIAB IMPB be slightly higher than the chondritic value, its core-mantle differentiation fO_2 would resemble that of other NC IMPBs, thus resulting in no anomalous enrichment of S. Note that, unlike other elements, S contents of the parent cores of IMPBs are not directly established from the measurements of iron meteorites and are rather determined indirectly from fractional crystallization models (*41*). Whether the anomalous enrichment of S in the IIAB IMPB is an artifact of the low fO_2 of core-mantle differentiation in its parent body or the high S content of its parent core based on fractional crystallization models requires further investigation.

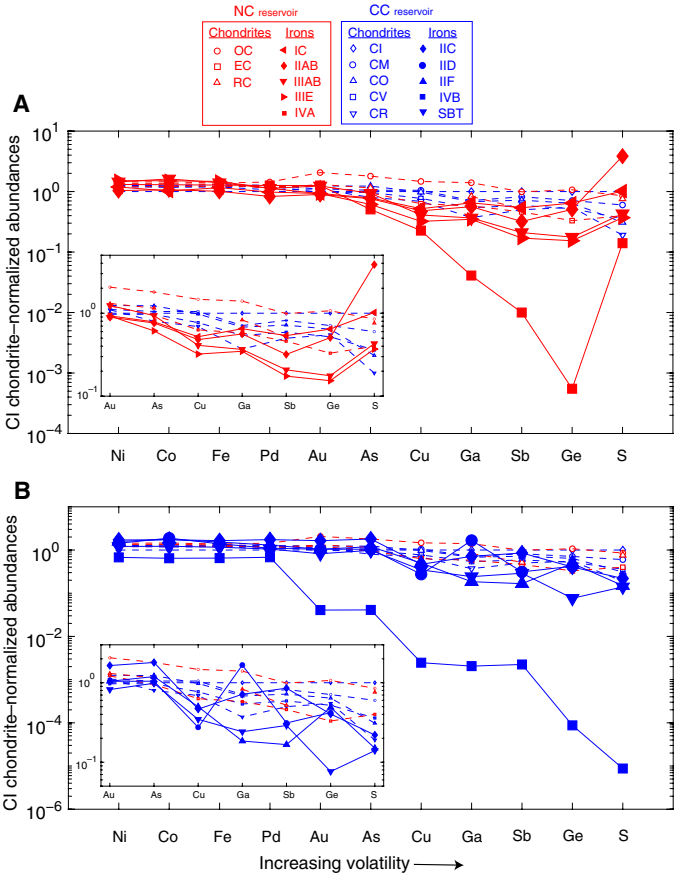

Fig. 1. Mean inventories of refractory elements (Ni, Co, Fe, and Pd) and MVEs (Au, As, Cu, Ga, Sb, Ge, and S) in NC (red) and CC (blue) IMPBs plotted as a function of elemental volatility (here, 50% T_C). The insets in (**A**) and (**B**) provide a magnified view of the MVE abundances in NC and CC IMPBs. MVE abundances in NC and CC IMPBs (except IVA and IVB) are within the range of chondrites, albeit with intra- and intergroup variations. In contrast, MVE-depleted IVA and IVB IMPBs show sloped MVE depletion patterns, with greater MVE depletion observed for the more volatile MVEs (except S for IVA). In addition, IVB IMPB also exhibits depletion of Ni, Co, Fe, and Pd compared to chondrites. Note that Au is known to have lower volatility in the metallic system (*40*, *55*) compared to the predictions of 50% T_C (*114*).

Broadly similar patterns are also apparent for MVE abundances in CC IMPBs (except IVB) (Fig. 1B and table S1). Au and As contents in IIC, IID, IIF, and SBT IMPBs are chondritic followed by a depletion trend toward the more volatile MVEs. Like NC IMPBs, each CC IMPB (except IVB) is depleted in Cu, Ga, Sb, Ge, and S by approximately fixed amounts compared to CI chondrites and does not follow the volatile depletion trend. Note that there is larger intragroup variability in the Cu, Ga, Sb, Ge, and S contents in CC IMPBs compared to NC IMPBs. This could in part be related to the differences in the crystallization processes (e.g., the formation of S-rich immiscible melts) within the parent cores of NC and CC IMPBs (*38*).

Unlike other NC and CC IMPBs, MVE contents in IVA and IVB IMPBs show monotonic volatile depletion with 50% T_C (Fig. 1, A and B). In the IVA IMPB, Au with chondritic abundance is the volatile-rich end-member and Ge is the most volatile-depleted element (~10^{-3} × CI). However, S does not follow the volatile depletion trend. It remains unclear how a core that was extremely depleted in all MVEs retained weight % level S. Sulfur may exhibit lower volatility than Cu, Ga, Sb, and Ge in environments where the precursor materials of the IVA IMPB condensed. For instance, S is less depleted than Cu, Ga, Sb, and Ge in the metal of CB chondrites (*55*), which likely condensed from an impact vapor plume (*56*, *57*). The volatility of S compared to other MVEs can be suppressed in such settings with high dust/gas ratios (*55*).

The IVB IMPB exhibits a more extreme volatile depletion than its IVA counterpart (Fig. 1, A and B). Au, unlike its chondritic abundance in the IVA IMPB, is depleted (10^{-2} × CI), and Ge shows an order of magnitude higher depletion (10^{-4} × CI). Unlike the IVA IMPB, S follows the volatile depletion trend since its parent core is predicted to be almost S free (*38*, *41*). It is noteworthy that, unlike all other NC and CC IMPBs, the IVB IMPB exhibits a depletion of relatively refractory elements such as Ni, Co, Fe, and Pd to a nearly equivalent extent (~0.67 × CI) (Fig. 1B). This observation suggests that, contrary to the predictions based on the HSE enrichment in IVB irons relative to CI chondrites (*33*), the parent core mass fraction (4%) of the IVB IMPB was not anomalously low compared to other CC IMPBs, which ranges from 7 to 18%. The unusual HSE enrichment in the IVB irons may be attributed to the loss of an early segregated S-rich, HSE-poor core component, analogous to ureilites (*58*, *59*), followed by the catastrophic destruction of its parent body (*60*).

The reconstructed P contents in all CC IMPBs and two NC IMPBs (IIIAB and IIIE) exhibit anomalous enrichment, whereas the rest of NC IMPBs display chondritic abundances (fig. S2, A and B). The main factor contributing to the anomalous enrichment in these IMPBs is the lithophile behavior of P within the estimated range of their fO_2 of core-mantle differentiation (fig. S1). It should be noted that the initial P content assigned to the parent cores in the fractional crystallization models can be up to an order of magnitude

higher than those measured in iron meteorites. For instance, the initial P content assigned to the IIC parent core in the fractional crystallization models is 2.2 to 3 wt % (*33*, *38*), whereas those measured in IIC iron meteorites are 0.3 wt % or lower (*61*). Considering the lithophile behavior of P, its anomalous enrichment in NC and CC IMPBs can be resolved only if the P contents in their parent cores are lower (up to ~0.01 to 0.3 wt %) than those assigned in the fractional crystallization models [~0.1 to 0.7 and 0.5 to 3 wt % for NC and CC parent cores, respectively; (*33*, *38*)]. It is important to highlight that since P is not a major element in the parent cores of IMPBs, the elemental compositions of the parent cores predicted by fractional crystallization models are not particularly sensitive to their initial P contents (see Materials and Methods for details). For instance, these models yield similar elemental abundances in the parent cores even when lower initial P contents are considered (fig. S3 and table S2).

We note that fractional crystallization models yield nonunique solutions for the chemical compositions of the parent cores of NC and CC IMPBs. These solutions depend on factors like the initial S content of the parent core and the composition of the first crystallized metal. Nonetheless, previous research has demonstrated that, even when these variable factors are considered, the elemental abundances show limited variation, typically within a standard deviation of less than 5% (*37*–*40*). Consequently, the estimated abundances of siderophile and chalcophile in NC and CC IMPBs presented in this study are robust and are not substantially affected by the variability in the results of fractional crystallization models.

DISCUSSION

The reconstructed bulk chemical compositions of NC IMPBs indicate a general classification into three categories—those with chondritic MVE contents (IC and IIAB), those with subchondritic MVEs (IIIAB and IIIE), and those with extremely low MVE contents (IVA) (Fig. 1A). The IC and IIAB IMPBs represent volatile-rich end-members, with MVE contents within the range of OCs, RCs, CO, CV, CK, and CR chondrites but lower than those of ECs, CI, and CM chondrites (Fig. 1A). In contrast, MVE contents of the IIIAB and IIIE IMPBs are lower (by a factor of ~2 to 5) than all classes of chondrites. Analogously, CC IMPBs also display a mix of MVE-rich (IIC, IID, IIF, and SBT) and MVE-poor (IVB) planetesimals. The IIC IMPB contains MVEs within the range of CO and CV chondrites but lower than CI and CM chondrites, while MVE contents in the IID, IIF, and SBT IMPBs are lower (by a factor of ~2 to 5) than all classes of chondrites (Fig. 1B). The IVA and IVB IMPBs from the NC and CC reservoirs, respectively, exhibit extreme volatile depletion (by factors of ~10 to 100 and ~100 to 1000, respectively) compared to all classes of chondrites. In summary, NC and CC IMPBs showcase no distinct differences in their MVE abundance patterns, signifying the presence of both volatile-rich and volatile-poor earliest-formed differentiated planetesimals in both the inner and outer regions of the solar protoplanetary disk.

Cause behind the MVE depletion of IVA and IVB irons

Does the presence of MVE-rich and MVE-poor NC IMPBs signify substantial variations in the MVE contents of primordial materials during the earliest stages of planetesimal formation in the inner disk? Or does it reflect secondary processing on the core compositions of planetesimals that accreted primordial materials with broadly similar MVE contents? If the first scenario is true, then the composition of the parent core of the IVA IMPB captures the accretion of MVE-poor primordial materials. However, if the second scenario is valid, then the MVE-depleted characteristics of IVA iron meteorites document a secondary stage of volatile loss from its parent core. This scenario undermines the reconstructed MVE-depleted bulk composition of its parent body as indicative of its primordial composition. Determining which of these scenarios is accurate holds important implications for gaining insights into the thermal structure of the inner disk, where the seeds of terrestrial planets formed, as well as understanding the fate of MVEs during the differentiation of planetesimals and during planetesimal collisions. Multiple lines of evidence support the second scenario:

1) The MVE depletion pattern analogous to the IVA parent core is also observed in that of the IVB (*32*, *38*) and several ungrouped CC irons (Chinga, Tishomingo, and Willow Grove) (*62*) emanating from the colder, outer region of the disk. The IVB irons and these ungrouped CC irons sample the most volatile-depleted cores, exhibiting an order of magnitude higher MVE depletion compared to the IVA irons.

2) Large variations in the metallographic cooling rates of iron meteorites from groups IVA and IVB and their Pd-Ag isotope systematics, along with the pyroxene geochemistry of IVA irons, indicate that their parent cores underwent volatile loss during vapor-metallic melt exchange (*60*, *63*–*69*). This exchange occurred either at the surfaces of stripped metallic cores or from the collisional fragments of cores formed after disruption of their parent bodies.

3) CB and CH chondrite metals, whose MVE depletion is linked to incomplete condensation in an impact plume formed after high-energy collisions between rocky bodies (*55*, *57*, *70*), exhibit MVE depletion patterns analogous to IVA and IVB irons as well as MVE-depleted ungrouped irons.

4) Carbon (C) and nitrogen (N) contents in the parent cores of NC and CC IMPBs (*34*, *71*) are correlated with the MVE contents (Fig. 2), with the IVA and IVB cores being the C- and N-depleted end-members. Given that the carriers of C and N (organics/ices) in the primordial materials are decoupled from those of siderophile MVEs (nebular metal) (*26*, *72*), the correlated depletion of MVEs and C-N in the parent cores of IVA and IVB IMPBs can only be explained if the planetesimals that accreted the most MVE-depleted materials also fortuitously accreted the most C- and N-poor materials, which is highly unlikely. A common volatile loss event presents a more straightforward explanation for this correlated depletion of MVEs and C-N in IVA and IVB groups.

5) The absence of a substantial difference in the oxidation states between NC and CC IMPBs suggests that the earliest-formed planetesimals in both the inner and outer Solar System accreted beyond the water snowline (*53*). This makes it improbable that the formation zone of the IVA parent body had temperatures high enough to not condense MVEs.

6) The IVA IMPB has a younger accretion and core formation age compared to other MVE-rich IMPBs such as IC, IIAB, and IIIAB (*15*, *42*). The IC and IIAB IMPBs—the MVE-rich end-members in the NC reservoir—have the oldest accretion ages (*42*). This calls into question the temporal evolution of temperature in the NC reservoir as a cause behind the volatile-depleted character of the IVA IMPB.

The collective evidence strongly supports the notion that the exceptionally volatile-depleted nature of IVA and IVB iron meteorites is a consequence of secondary volatile loss event(s) from their core materials rather than an incomplete condensation signature. Effective

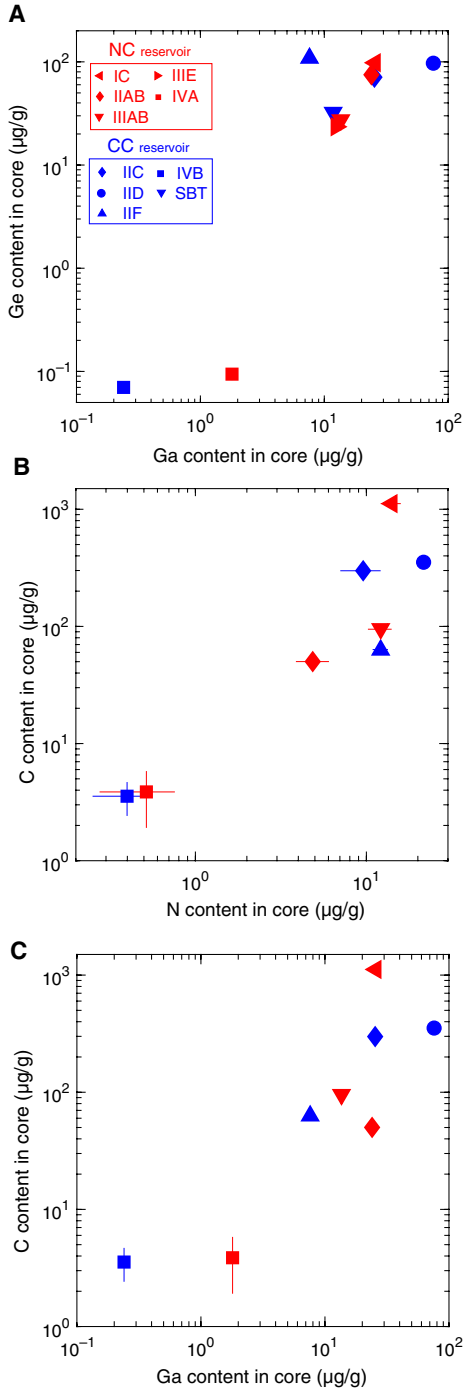

Fig. 2. Abundances of Ge versus Ga, C versus N, and C versus Ga in the parent cores of IMPBs. (**A**) Ga and Ge abundances in the parent cores broadly show positive correlation across NC and CC IMPBs, with IVA and IVB being the volatile-depleted end-members. (**B**) C and N abundances also show similar correlation. (**C**) C and Ga, with distinct primordial carries, are also correlated with the parent cores of IVA and IVB being the volatile-depleted end-members. Data sources: Ge and Ga, (*38*, *40*); C and N, (*71*). Errors bars for C and N represent 1σ deviation from the mean. NC and CC IMPBs are shown in red and blue colors, respectively.

volatile loss is more likely if the parent bodies were disrupted before the solidification of their cores or the collisions were energetic enough to cause large-scale melting and vaporization (*68*). The Pd-Ag closure age of IVA irons constrains the disruption event(s) to have occurred between ~3 and 9 Myr after CAIs, i.e., when the cores were still molten (*73*). The precise mechanism behind the volatile loss remains unclear, as research delving into its underlying causes is limited. Large variations in metallographic cooling rates (*60*, *63*, *64*), along with Pd-Ag isotopic data (*65*, *66*) from IVA and IVB iron meteorites, have been used to hypothesize that the evaporative loss of MVEs could have occurred from exposed molten cores subsequent to mantle stripping (*69*). While substantial mass-dependent isotopic variations are anticipated during simple evaporative loss during the degassing of metallic magma into a vacuum (e.g., by Rayleigh fractionation), no such pronounced isotopic variations have been identified for Ge (*74*, *75*), Cu (*76*), Zn (*77*), and S (*78*) isotopes in IVA and IVB irons. These measurements do not support the evaporative loss of MVEs from the parent cores of IVA and IVB groups occurring through a kinetic regime (*74*, *76*, *77*). Isotopic fractionation of MVEs during evaporation can be mitigated if volatile loss occurred under near-equilibrium conditions (*79*). While degassing can cause chemical fractionation of elements, incomplete recondensation in a kinetic regime within an impact-generated vapor cloud—similar to what has been postulated for the CB chondrites (*55*–*57*)—offers an alternative explanation for volatility-driven depletion with limited isotopic fractionation (*80*). Further research is required to better understand the underlying cause of volatile loss from the parent cores of IVA and IVB irons.

In summary, IVA and IVB iron meteorites are remnants of core materials that underwent MVE loss after disruptive collision of their parent bodies (*39*, *67*, *68*, *81*). This suggests that the MVE contents of the IVA and IVB parent cores, and consequently of their parent bodies, were much higher and were likely within the range of other volatile-bearing NC and CC IMPBs, respectively, forming in the same region of the disk and within similar timescales (*69*). Whether the IVA IMPB accreted primordial materials as MVE rich as IC and IIAB IMPBs or relatively MVE depleted akin to IIIAB and IIIE IMPBs remains unknown. Variations in the metallographic cooling rates coupled with Pd-Ag isotope systematics of IIIAB iron meteorites suggest that their cores also experienced some degree of secondary volatile loss (*65*, *73*, *82*), although not as marked as that of the IVA and IVB cores. Therefore, it is plausible that the MVE contents of the parent cores of all NC IMPBs, and as a consequence, of the primordial materials accreted by their parent bodies, were at least comparable to those of volatile-rich IC and IIAB IMPBs. This implies that the "first-generation" earliest-formed planetesimals in the NC reservoir were remarkably MVE rich, and many of these planetesimals (e.g., IC, IIAB, IIIAB, and IIIE IMPBs) even retained a bulk of their MVE inventory during the early collisional history of the Solar System.

Consequences of the MVE inventory of NC IMPBs

The presence of MVEs and highly volatile elements such as C and N (*34*–*36*, *71*, *83*–*85*) along with the relatively oxidized characteristics of NC IMPBs (*53*) indicates that the earliest-formed planetesimals in the NC reservoir, akin to the parent bodies of NC and CC chondrites as well as NC primitive achondrites, accreted volatile-bearing materials containing MVEs, C, N, and water-ice. The cumulative weight of this evidence argues against the notion that incomplete condensation from a hot nebular cloud was the main driver of MVE depletion in the earliest-formed NC planetesimals, including Vesta and angrite

parent body (APB). Therefore, contrary to predictions from astrophysical (*14*, *21*) and geochemical models (*5*, *19*), the earliest NC planetesimals did not form by accreting refractory-enriched materials. Instead, their volatile-bearing characteristics suggest growth in a relatively colder region of the disk, potentially beyond the water snowline (*53*).

The MVE-bearing character of the parent cores of NC IMPBs (e.g., groups IC, IIAB, IIIAB, and IIIE) also suggests that the earliest-formed planetesimals did not experience substantial MVE loss from magma oceans during core formation. Since Vesta and APB formed and differentiated at similar or later timescales, it is unlikely that volatile loss during magma ocean degassing from the surface of their parent bodies, as previously postulated (*22*, *24*), was the primary cause behind the bulk MVE depletion of their parent bodies. This agrees with current geophysical models that predict that ^{26}Al decay–led melting in the earliest planetesimals occurred beneath unmolten surfaces in the absence of surficial magma oceans (*86*–*88*). This pushes the timeline of volatile depletion in the building blocks of terrestrial planets from the differentiation stage of planetesimals to the collisional phase of planetary growth. Volatile loss during high-energy impacts in the chaotic history of the early Solar System, as has been postulated for the IVA and IVB irons (*39*, *60*, *63*, *64*, *66*–*68*), MVE-depleted ungrouped irons (*62*), CB chondrites (*55*–*57*), and angrites and HEDs (*2*, *28*–*30*), could therefore be considered as a general mechanism for volatile depletion in the building blocks of terrestrial planets.

In addition to siderophile MVEs, NC iron meteorites also contain nominally lithophile MVEs like Cr and Cl (*31*, *89*). This implies that NC IMPBs, beyond accreting siderophile MVEs covering a wide range of 50% T_C, must also have accreted lithophile MVEs, including alkali elements. The presence of alkalis like Na and K in NC IMPBs plays a major role in shaping several key chemical and physical properties during their thermal evolution. These include the silicate solidus, composition and viscosity of the first-formed silicate melts, fate of ^{26}Al (primary heat source) during partial melting, and the mechanism and timing of core formation (*10*, *11*, *90*, *91*). The abundance of Ga (exhibiting a 50% T_C similar to Na and K) in IC and IIAB IMPBs indicates that Na and K abundances in NC IMPBs were in the range of ~0.6 × CI. This is in agreement with the chondritic silicate lithology of group IAB-MG irons (a nonmagmatic NC iron meteorite group), which are known to sample a volatile-rich chondritic precursor (*92*). This implies that the earliest-formed inner Solar System planetesimals, consistent with primitive achondrite and chondrite parent bodies (*9*–*11*), were not depleted in alkali elements. Consequently, the extremely low Rb/Sr and K/U ratios in HEDs and angrites likely stem from secondary volatile loss processes and not from the accretion of alkali-poor, refractory-rich materials.

Origin of MVEs in Earth and Mars

Isotopic signatures of Cr, Ti, and O suggest that Earth and Mars primarily accreted materials originating from the NC reservoir (*6*, *7*). Earth acquired only ~4% of its mass from CC reservoir–derived materials (*6*), and Mars received an even smaller contribution (*93*). Isotopic compositions of MVEs also indicate that majority of their mass in Earth and Mars was sourced from the NC reservoir. For example, NC reservoir–derived materials contributed to ~70% of Zn (*94*–*96*) and ~90% of K (*97*) inventory in Earth, whereas almost the entire Zn inventory in Mars was sourced from the NC reservoir (*93*, *98*).

Planet formation models predict that the seeds of terrestrial planets began to form almost at the onset of Solar System formation (*14*–*16*). Should the earliest-formed planetesimals in the NC reservoir based on the projections of HEDs and angrites have accreted extremely MVE-depleted materials or efficiently lost their MVE inventory during differentiation or impacts (*5*, *19*, *22*, *24*), it would present a challenge to establish the MVE inventory of Earth and Mars primarily from NC reservoir–derived materials. This is particularly problematic for Mars, which grew rapidly within the first few million years after CAIs (*99*) and accreted its entire mass, including those of MVEs, almost exclusively from the NC reservoir (*93*, *98*). The reconstructed MVE inventory of NC IMPBs in this study presents a straightforward solution to this problem as it indicates that the earliest-formed planetesimals in the NC reservoir not only accreted MVE-bearing materials, but they could also retain a substantial fraction of their MVE inventory during early Solar System processes such as planetesimal differentiation. Consequently, the MVE-bearing characteristics of NC IMPBs link the MVE inventory of terrestrial planets, as predicted by their isotopic compositions (*93*–*98*), to the earliest-formed planetesimals in the inner Solar System.

Although both Earth and Mars grew by almost exclusively accreting inner Solar System planetesimals, Earth exhibits a more pronounced depletion in MVEs compared to Mars (Fig. 3). This presents a conundrum because, in addition to its larger size, Earth received a greater share of its mass, including the MVE inventory, from the volatile-rich CC reservoir (*6*). The heightened MVE depletion in Earth compared to Mars could be tied to the differences in their growth histories. Mars, as a stranded planetary embryo, accreted almost all of its mass very early in the Solar System history (*99*). In contrast, Earth had a protracted growth period, accumulating mass over tens of millions of years. Pd-Ag systematics of iron meteorites suggest that collision-related volatile losses took place in an energetic inner Solar System between ~4 and 16 Myr after CAIs, coinciding with the cessation of the damping effect of the nebular gas (*65*, *66*, *73*). Since Mars formed well before this time frame, it predominantly grew from volatile-rich

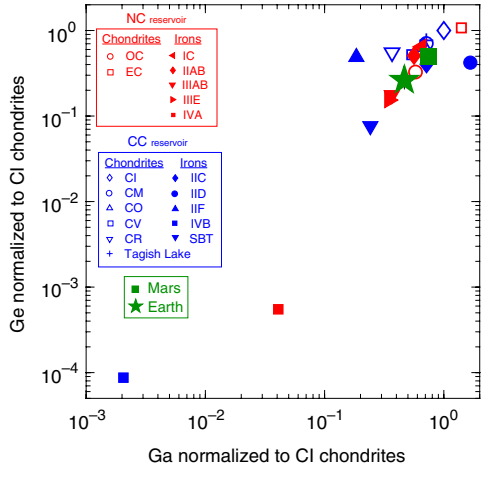

Fig. 3. Variation in the CI chondrite–normalized abundances of Ge and Ga across bulk IMPBs, chondrites, bulk Earth, and bulk Mars. Ga and Ge abundances are positively correlated across all rocky bodies. Ge and Ga abundances in IC, IIAB, IIC, and IID IMPBs plot in the chondritic range. Whereas IIF, IIIAB, IIIE, and SBT IMPBs have subchondritic Ge and/or Ga contents, IVA and IVB IMPBs are extremely Ge and Ga depleted. The Ge and Ga abundances in bulk Mars plot within the range of MVE-rich IC and IIAB IMPBs, whereas bulk Earth is more Ge and Ga depleted. Data sources: bulk IMPBs, present study; chondrites, (*9*, *115*); bulk Mars, (*116*); bulk Earth, (*117*).

"first-generation" NC planetesimals, akin to IC and IIAB IMPBs, that largely avoided collision-related volatile losses. In contrast, a substantial proportion of volatile-depleted planetesimals, akin to partially degassed IIIAB and IIIE IMPBs and extensively degassed IVA IMPBs, could have contributed to Earth's growth because of its protracted formation. The accretion of Earth via a mixture of IC, IIAB, IIIAB, and IIIE IMPB–like volatile-bearing and IVA and IVB IMPB–like volatile-depleted planetesimals, with flat and sloping MVE patterns, respectively, could also explain the hockey stick–like MVE depletion pattern in bulk silicate Earth (*100*).

Despite Earth's MVE depletion, its MVEs exhibit chondritic isotopic compositions. This observation has been used to suggest that incomplete nebular condensation, rather than volatile loss during evaporation, caused MVE depletion in terrestrial planets because partial evaporative loss from Earth's building blocks is expected to result in detectable isotopic fractionation (*5*). However, near-chondritic isotopic ratios of Ge (*74*), Cu (*76*), and Zn (*77*) isotopes in iron meteorite groups with varying MVE abundances (e.g., IC and IIAB versus IIIAB and IIIE versus IVA) suggest that the core materials experienced volatile loss in the early Solar System without notable isotopic fractionation. Because of negligible isotopic fractionation at high temperatures relevant for metal-silicate equilibration (*35*, *101*), the isotopic compositions of MVEs in the cores should closely represent the bulk isotopic signatures of their parent bodies. Thus, despite variable volatile losses, bulk planetesimals retained chondritic isotopic ratios. The growth of Earth and other terrestrial planets via the accretion of "first-, second-, and subsequent-generation" planetesimals and planetary embryos can, therefore, explain their MVE depletion while retaining near-chondritic isotopic ratios of MVEs. Consequently, the MVE depletion in terrestrial planets of our Solar System is linked to the protracted history of volatile depletion during their collisional growth and is divorced from incomplete condensation in the solar protoplanetary disk and MVE loss during magma ocean degassing.

MATERIALS AND METHODS

Metal-silicate partition coefficients

Quantification of elemental distribution between metallic and silicate melts during core-mantle differentiation is achieved through the application of multivariate linear regression equations derived from high pressure-temperature experimental data on metal-silicate partitioning. Recent studies have capitalized on the extensive repository of experimental data on metal-silicate partitioning amassed over the preceding decades to formulate multivariate linear regression equations for all siderophile and chalcophile elements that are present in iron meteorites (*46*–*49*, *51*).

For the MVEs, we use the following equations to constrain the elemental partitioning during core-mantle differentiation in IMPBs.

Mo, P, Ga, and Ge

$$\begin{aligned}\log D_i = a + b\,(\Delta\mathrm{IW}) + c_1\,(\mathrm{MgO}) + c_2\,(\mathrm{SiO_2}) + c_3\,(\mathrm{Al_2O_3}) \\ + c_4\,(\mathrm{CaO}) + c_5\,(\mathrm{FeO}) + d\,(1/T) + e\,(P/T) + f\ln(1-X_\mathrm{S}) \\ + g\ln(1-X_\mathrm{C}) + h\ln(1-X_\mathrm{Ni})\end{aligned} \quad (2)$$

Ni, Co, and Cu

$$\begin{aligned}\log D_i = a + b\,(\Delta\mathrm{IW}) + c\,(\mathrm{NBO/T}) + d\,(1/T) + e\,(P/T) \\ + f\ln(1-X_\mathrm{S}) + g\ln(1-X_\mathrm{C}) + h\ln(1-X_\mathrm{Ni})\end{aligned} \quad (3)$$

Au and As

$$\begin{aligned}\ln D_i = a + b\,(\Delta\mathrm{IW}) + c\,(\mathrm{NBO/T}) + d\,(1/T) + e\,(P/T) \\ + f\ln(1-X_\mathrm{S}) + g\ln(1-X_\mathrm{C}) + h\ln(1-X_\mathrm{Ni})\end{aligned} \quad (4)$$

where a, d, and e are coefficients related to the expansion of the Gibbs free energy term. T is the temperature in kelvin, and P is the pressure in gigapascal. b is a coefficient related to the oxygen fugacity (fO_2) relative to the iron-wüstite (IW) buffer. The silicate composition is represented either in the form of separate mole oxide fractions (Eq. 2) and c_1, c_2, c_3, c_4, and c_5, which are the corresponding coefficients, or by NBO/T (Eqs. 3 and 4), a measure of degree of silicate melt polymerization that is expressed as total nonbridging oxygens per tetrahedral cations {NBO/T = [2 × Total O]/T − 4, where T = Si + Ti + Al + Cr + P}. Coefficients f, g, and h are related to the effect of dissolved S, C, and Ni in metallic liquid. X_S, X_C, and X_Ni are the molar fractions of S, C, and Ni in the metallic phase. The coefficients and relevant references for Eqs. 2 to 4 are reported in tables S3 and S4.

For the HSEs, we use the following equation from (*46*) to constrain the elemental partitioning during core-mantle differentiation in IMPBs

$$\log K_\mathrm{D} = \log\left[D_i/\left(D_\mathrm{Fe}\right)^{n/2}\right] = a + b\,(1/T) + c\,(P/T) \quad (5)$$

where n = 4, 3, 2, 4, 4, and 4 for Ru, Rh, Pd, Re, Ir, and Pt, respectively. Note that, unlike Eqs. 2 to 4, the above equation lacks terms associated with the compositions of metallic and silicate melts. This omission arises from the limited constraints on the individual effects of these terms. However, it is anticipated that this omission will not markedly impact the outcomes of the study. This is attributed to the highly siderophile nature of Ru, Rh, Pd, Re, Ir, and Pt, indicating that these elements likely segregated predominantly into the cores regardless of the specific conditions governing core-mantle differentiation in each IMPB.

For S, we use the following equation reported in (*50*)

$$\begin{aligned}\log D_\mathrm{S} = -3.30 + 3000\,(1/T) + 33\,(P/T) \\ + \ln\left(X_\mathrm{FeO}^\mathrm{silicate}\right) - \ln C_\mathrm{S} + 14\left(1-X_\mathrm{O}\right)\end{aligned} \quad (6)$$

where $X_\mathrm{FeO}^\mathrm{silicate}$ is the mole reaction of FeO in the silicate melt, and X_O is the molar fractions of O in the metallic phase (0 in the case of IMPBs). C_S is the value of sulfide capacity of the silicate melt and is calculated as a function of silicate melt composition following the framework in (*102*).

For Sb, we used the following equation reported in (*52*)

$$\begin{aligned}\log K_\mathrm{D} = \log\left[D_\mathrm{Sb}/\left(D_\mathrm{Fe}\right)^{n/2}\right] = -5.41 + 14870\,(1/T) \\ + 193\,(P/T) - \log\gamma_\mathrm{Sb}^0 + \varepsilon_\mathrm{Sb}^\mathrm{Sb}\log\left(1-X_\mathrm{Sb}\right) \\ + 10.48\log\left(1-X_\mathrm{S}\right) + (n/2-1)\,\varepsilon_\mathrm{S}^\mathrm{S}\left[X_\mathrm{S}\cdot\log\left(1-X_\mathrm{S}\right)\right]\end{aligned} \quad (7)$$

where n = 3, and γ_Sb^0 is the activity coefficient, which accounts for nonideal interactions between the components in the metallic phase (*103*) and calculated using the "Online Metal Activity Calculator" (https://norrisau.org/expet/metalact/). Values of individual parameters are obtained using Eqs. 2 to 7.

Pressure (P)

Thermal models, coupled with metallographic cooling rates in iron meteorites, suggest that IMPBs had radii ranging between 250 and 500 km (*34*, *64*, *87*). These estimates are consistent with conventional projections for the radii of other early-accreting planetesimals, such as 4Vesta (the presumed parent body of HEDs) and APB (*104*, *105*). The equilibration pressure for metal-silicate melt equilibration within 4Vesta and APB is estimated to be around 0.1 GPa (*48*, *106*). Given the similar sizes of IMPBs, it is reasonable to infer that the pressures at which metal-silicate melt equilibration occurred would broadly fall within a comparable range to those of Vesta and APB. Because of the lack of precise constraints for each IMPB, analogous to previous studies (*34*, *35*), we used a fixed equilibration pressure of 0.1 GPa for metal-silicate equilibration. Under these relatively shallow pressures, minor variations in the pressure of metal-silicate equilibrium are not anticipated to substantially alter the values of $D_i^{\text{metal/silicate}}$ for the siderophile and chalcophile elements of interest in this study.

Temperature (T)

The surface tension dynamics between O-poor metallic melt, relevant for the composition of the parent cores of IMPBs, and the solid silicate matrix suggest that the percolation-driven core formation in IMPBs is inefficient (*90*). It is anticipated that metallic melts can only migrate to form the core under the circumstances where the silicate matrix has experienced considerable melting (>40 vol %) to reach magma ocean–like conditions (*107*). According to the melting relationships of chondritic lithologies, temperatures required for substantial silicate melting should exceed 1450°C (*108*, *109*). Consequently, in agreement with previous studies that constrain the temperature of core-mantle differentiation in IMPBs (*32*, *34*, *42*, *87*), we adopted a fixed temperature of 1600°C. Analogous to pressure considerations, minor variations in the temperature of metal-silicate equilibrium are not expected to markedly alter the values of $D_{\text{i}}^{\text{metal/silicate}}$ for the siderophile and chalcophile elements of interest in this study.

Oxygen fugacity (fO_2)

In the case of each IMPB, we relied on the metal-silicate equilibration fO_2 values documented in a recent study (*53*), determined from the Fe/Ni ratios observed in the parent cores of IMPBs.

Composition of metal

We used the C content of the equilibrating metal from the reported values in (*71*), while for Ni and S, we relied on the values documented in (*38*, *40*).

Composition of silicates

Given the shared origins of ordinary chondrites and NC IMPBs from the inner Solar System reservoir (*42*) and their comparable oxidation states (*53*), we used the composition data of ordinary chondrites from (*110*) to establish the chemical composition of silicate melts in Eqs. 2 to 4. Likewise, for CC IMPBs, we relied on the chemical compositions of CC chondrites as documented in (*110*).

Sensitivity of the results of the fractional crystallization models to the initial P content of the parent core

We want to emphasize that since P is a minor element in the parent cores of IMPBs, the elemental concentrations predicted for the parent cores by fractional crystallization models are not particularly sensitive to their initial P contents. Here, we demonstrate that using lower P contents, which aligns the bulk compositions of IMPBs with chondritic compositions, in fractional crystallization models does not substantially alter the compositions of the parent cores. The fractional crystallization modeling methods are described in the literature (*37*, *41*). We provide a summary below. The model uses small-step batch crystallization to simulate the fractional crystallization of metallic melts. Within metallic melts, the partition coefficients of trace elements undergo changes as S and P contents vary during crystallization.

The equilibrium batch crystallization is a simple mass balance between the phase fields

$$\frac{C_L}{C_i} = \frac{1}{\left(1 - f + f \times D_E\right)} \tag{8}$$

In Eq. 8, C_i, C_L, f, and D_E represent the bulk composition of the liquid, the bulk composition of the remaining liquid, the crystallization step, and the partition coefficient of an element between solid and liquid metal, respectively. The models are set to have a constant f of 0.001 for each mass step. The concentration of an element in the solid (C_s) that is derived from each mass step is calculated using the bulk composition of the remaining liquid and the partition coefficient of the element in that step

$$C_s = D_E \times C_L \tag{9}$$

The partition coefficient of an element is influenced by the S and P contents of the liquid and varies at each small step. D_E is parameterized using Eq. 10 (*41*)

$$D_E = D_0 \times (\text{Fe domains})^{\beta} \tag{10}$$

D_0 is the partition coefficient of an element in the S- and P-free system. β is a constant specific to an element related to S and P in the liquid. Fe domains represent the fraction of free Fe atoms available in the liquid (*111*). Fe domains in the Fe-Ni-S-P system were calculated using Eq. 11, and β_{S+P} of an element in the Fe-Ni-S-P system was calculated using Eq. 12 (*112*)

$$\text{Fe domains} = \frac{1 - 2X_{\text{S}} - 4X_{\text{P}}}{1 - X_{\text{S}} - 3X_{\text{P}}} \tag{11}$$

$$\beta_{S+P} = \left[\frac{2X_{\text{S}}}{\left(2X_{\text{S}} + 4X_{\text{P}}\right)}\right]\beta_{\text{S}} + \left[\frac{4X_{\text{P}}}{\left(2X_{\text{S}} + 4X_{\text{P}}\right)}\right]\beta_{\text{P}} \tag{12}$$

X_{S} and X_{P} are the molar fractions of S and P in the liquid, respectively. β_{S} and β_{P} are the β values for each element in the Fe-S and Fe-P systems, respectively.

It is hypothesized that the scattered interelement trends of group IIIAB are caused by the equilibrium mixing of fractional-crystallization solid and trapped-melt solid (*113*), which is called the trapped-melt model. A recently revised version of the trapped-melt model considers the formation of troilite in the trapped melt (*37*). The relationship between the trapped melt ($C_{\text{Trapped melt}}$) and the solid ($C_{\text{Trapped melt solid}}$) that crystallized from the trapped melt can be expressed using Eq. 13

$$C_{\text{Trapped melt solid}} = \frac{C_{\text{Trapped melt}}}{1 - x} \tag{13}$$

where x denotes the mass fraction of the trapped melt that solidifies to form troilite.

For CC groups, we use the fractional crystallization models to calculate the composition of the parent core using the maximum P content allowed in the core based on its metal-silicate partition coefficient (0.017 and 0.052 wt % for groups IIC and IID, respectively) and a P-free core and compare them with the values predicted in (*40*) (table S2). Using low P contents and P-free conditions reproduces the interelement trends of these groups predicted by previous studies (*38*, *40*) (fig. S3). This analysis shows that the estimated abundances of siderophile and chalcophile in NC and CC IMPBs presented in this study are robust and are not substantially affected by the variability in the initial P content of the fractional crystallization models.

Supplementary Materials

This PDF file includes:

Figs. S1 to S3
Tables S1 to S4

REFERENCES AND NOTES

1. H. Palme, H. O'Neill, *Cosmochemical Estimates of Mantle Composition* (Elsevier Ltd., ed. 2, 2013), vol. 3.
2. A. N. Halliday, D. Porcelli, In search of lost planets – The paleocosmochemistry of the inner solar system. *Earth Planet. Sci. Lett.* **192**, 545–559 (2001).
3. N. Dauphas, N. X. Nie, M. Blanchard, Z. J. Zhang, H. Zeng, J. Y. Hu, M. Meheut, C. Visscher, R. Canup, T. Hopp, The extent, nature, and origin of K and Rb depletions and isotopic fractionations in earth, the moon, and other planetary bodies. *Planet. Sci. J.* **3**, 29 (2022).
4. D. W. Mittlefehldt, Volatile degassing of basaltic achondrite parent bodies: Evidence from alkali elements and phosphorus. *Geochim. Cosmochim. Acta* **51**, 267–278 (1987).
5. P. A. Sossi, I. L. Stotz, S. A. Jacobson, A. Morbidelli, H. St, C. O'Neill, Stochastic accretion of the Earth. *Nat. Astron.* **6**, 951–960 (2022).
6. C. Burkhardt, F. Spitzer, A. Morbidelli, G. Budde, J. H. Render, T. S. Kruijer, T. Kleine, Terrestrial planet formation from lost inner solar system material. *Sci. Adv.* **7**, 7601 (2021).
7. N. Dauphas, The isotopic nature of the Earth's accreting material through time. *Nature* **541**, 521–524 (2017).
8. M. K. Weisberg, M. Kimura, The unequilibrated enstatite chondrites. *Chem. Erde* **72**, 101–115 (2012).
9. C. M. O. D. Alexander, Quantitative models for the elemental and isotopic fractionations in the chondrites: The non-carbonaceous chondrites. *Geochim. Cosmochim. Acta* **254**, 246–276 (2019).
10. M. Collinet, T. L. Grove, Formation of primitive achondrites by partial melting of alkali-undepleted planetesimals in the inner solar system. *Geochim. Cosmochim. Acta* **277**, 358–376 (2020).
11. M. Collinet, T. L. Grove, Widespread production of silica- and alkali-rich melts at the onset of planetesimal melting. *Geochim. Cosmochim. Acta* **277**, 334–357 (2020).
12. D. W. Mittlefehldt, Asteroid (4) Vesta: I. The howardite-eucrite-diogenite (HED) clan of meteorites. *Chem. Erde* **75**, 155–183 (2015).
13. K. Keil, Angrites, a small but diverse suite of ancient, silica-undersaturated volcanic-plutonic mafic meteorites, and the history of their parent asteroid. *Chemie der Erde* **72**, 191–218 (2012).
14. A. Morbidelli, K. Baillié, K. Batygin, S. Charnoz, T. Guillot, D. C. Rubie, T. Kleine, Contemporary formation of early Solar System planetesimals at two distinct radial locations. *Nat. Astron.* **6**, 72–79 (2022).
15. T. S. Kruijer, M. Touboul, M. Fischer-Godde, K. R. Bermingham, R. J. Walker, T. Kleine, Protracted core formation and rapid accretion of protoplanets. *Science* **344**, 1150–1154 (2014).
16. S. J. Weidenschilling, Initial sizes of planetesimals and accretion of the asteroids. *Icarus* **214**, 671–684 (2011).
17. N. Sugiura, W. Fujiya, Correlated accretion ages and ε 54 Cr of meteorite parent bodies and the evolution of the solar nebula. *Meteorit. Planet. Sci.* **49**, 772–787 (2014).
18. T. Kleine, U. Hans, A. J. Irving, B. Bourdon, Chronology of the angrite parent body and implications for core formation in protoplanets. *Geochim. Cosmochim. Acta* **84**, 186–203 (2012).
19. F. L. H. Tissot, M. Collinet, O. Namur, T. L. Grove, The case for the angrite parent body as the archetypal first-generation planetesimal: Large, reduced and Mg-enriched. *Geochim. Cosmochim. Acta* **338**, 278–301 (2022).
20. U. Hans, T. Kleine, B. Bourdon, Rb–Sr chronology of volatile depletion in differentiated protoplanets: BABI, ADOR and ALL revisited. *Earth Planet. Sci. Lett.* **374**, 204–214 (2013).
21. A. Izidoro, R. Dasgupta, S. N. Raymond, R. Deienno, B. Bitsch, A. Isella, Planetesimal rings as the cause of the Solar System's planetary architecture. *Nat. Astron.* **6**, 357–366 (2022).
22. K. Zhu, P. A. Sossi, J. Siebert, F. Moynier, Tracking the volatile and magmatic history of Vesta from chromium stable isotope variations in eucrite and diogenite meteorites. *Geochim. Cosmochim. Acta* **266**, 598–610 (2019).
23. E. A. Pringle, F. Moynier, P. S. Savage, J. Badro, J.-A. Barrat, Silicon isotopes in angrites and volatile loss in planetesimals. *Proc. Natl. Acad. Sci. U.S.A.* **111**, 17029–17032 (2014).
24. B. Wang, F. Moynier, Y. Hu, Rubidium isotopic compositions of angrites controlled by extensive evaporation and partial recondensation. *Proc. Natl. Acad. Sci. U.S.A.* **121**, e2311402121 (2024).
25. M. Schönbächler, R. W. Carlson, M. F. Horan, T. D. Mock, E. H. Hauri, Heterogeneous accretion and the moderately volatile element budget of earth. *Science* **328**, 884–887 (2010).
26. C. M. O. Alexander, An exploration of whether Earth can be built from chondritic components, not bulk chondrites. *Geochim. Cosmochim. Acta* **318**, 428–451 (2022).
27. N. Wu, J. Farquhar, J. W. Dottin, N. Magalhães, Sulfur isotope signatures of eucrites and diogenites. *Geochim. Cosmochim. Acta* **233**, 1–13 (2018).
28. I. S. Sanders, E. R. Scott, "The chronology of basaltic meteorites and the history of their parent bodies," in *Workshop on the Chronology of Meteorites and the Early Solar System* (2007), pp. 147–148.
29. P. A. Bland, G. K. Benedix, "Volatile depletion: Constraints from differentiated meteorites," in *69th Annual Meteoritical Society Meeting* (2006).
30. G. W. Lugmair, S. J. G. Galer, Age and isotopic relationships among the angrites Lewis Cliff 86010 and Angra dos Reis. *Geochim. Cosmochim. Acta* **56**, 1673–1694 (1992).
31. J. I. Goldstein, E. R. D. Scott, N. L. Chabot, Iron meteorites: Crystallization, thermal history, parent bodies, and origin. *Chem. Erde* **69**, 293–325 (2009).
32. A. J. Campbell, M. Humayun, Compositions of group IVB iron meteorites and their parent melt. *Geochim. Cosmochim. Acta* **69**, 4733–4744 (2005).
33. C. D. Hilton, R. D. Ash, R. J. Walker, Chemical characteristics of iron meteorite parent bodies. *Geochim. Cosmochim. Acta* **318**, 112–125 (2022).
34. D. S. Grewal, J. D. Seales, R. Dasgupta, Internal or external magma oceans in the earliest protoplanets – Perspectives from nitrogen and carbon fractionation. *Earth Planet. Sci. Lett.* **598**, 117847 (2022).
35. D. S. Grewal, T. Sun, S. Aithala, T. Hough, R. Dasgupta, L. Y. Yeung, E. A. Schauble, Limited nitrogen isotopic fractionation during core-mantle differentiation in rocky protoplanets and planets. *Geochim. Cosmochim. Acta* **338**, 347–364 (2022).
36. M. M. Hirschmann, E. A. Bergin, G. A. Blake, F. J. Ciesla, J. Li, Early volatile depletion on planetesimals inferred from C–S systematics of iron meteorite parent bodies. *Proc. Natl. Acad. Sci. U.S.A.* **118**, e2026779118 (2021).
37. N. L. Chabot, B. Zhang, A revised trapped melt model for iron meteorites applied to the IIIAB group. *Meteorit. Planet. Sci.* **57**, 200–227 (2022).
38. B. Zhang, N. L. Chabot, A. E. Rubin, Compositions of carbonaceous-type asteroidal cores in the early solar system. *Sci. Adv.* **8**, 5781 (2022).
39. A. E. Rubin, B. Zhang, N. L. Chabot, IVA iron meteorites as late-stage crystallization products affected by multiple collisional events. *Geochim. Cosmochim. Acta* **331**, 1–17 (2022).
40. B. Zhang, N. L. Chabot, N. L. Chabot, Compositions of iron-meteorite parent bodies: Constraints on the structure of the protoplanetary disk. *Proc. Natl. Acad. Sci. U.S.A.* **121**, e2306995121 (2024).
41. N. L. Chabot, Sulfur contents of the parental metallic cores of magmatic iron meteorites. *Geochim. Cosmochim. Acta* **68**, 3607–3618 (2004).
42. T. S. Kruijer, C. Burkhardt, G. Budde, T. Kleine, Age of Jupiter inferred from the distinct genetics and formation times of meteorites. *Proc. Natl. Acad. Sci. U.S.A.* **114**, 6712–6716 (2017).
43. F. Spitzer, C. Burkhardt, F. Nimmo, T. Kleine, Nucleosynthetic Pt isotope anomalies and the Hf-W chronology of core formation in inner and outer solar system planetesimals. *Earth Planet. Sci. Lett.* **576**, 117211 (2021).
44. D. S. Grewal, R. Dasgupta, T. Hough, A. Farnell, Rates of protoplanetary accretion and differentiation set nitrogen budget of rocky planets. *Nat. Geosci.* **14**, 369–376 (2021).
45. D. S. Grewal, R. Dasgupta, S. Aithala, The effect of carbon concentration on its core-mantle partitioning behavior in inner Solar System rocky bodies. *Earth Planet. Sci. Lett.* **571**, 117090 (2021).
46. U. Mann, D. J. Frost, D. C. Rubie, H. Becker, A. Audétat, Partitioning of Ru, Rh, Pd, Re, Ir and Pt between liquid metal and silicate at high pressures and high temperatures - Implications for the origin of highly siderophile element concentrations in the Earth's mantle. *Geochim. Cosmochim. Acta* **84**, 593–613 (2012).
47. E. S. Steenstra, N. Rai, J. S. Knibbe, Y. H. Lin, W. van Westrenen, New geochemical models of core formation in the Moon from metal–silicate partitioning of 15 siderophile elements. *Earth Planet. Sci. Lett.* **441**, 1–9 (2016).
48. E. S. Steenstra, A. B. Sitabi, Y. H. Lin, N. Rai, J. S. Knibbe, J. Berndt, S. Matveev, W. van Westrenen, The effect of melt composition on metal-silicate partitioning of siderophile elements and constraints on core formation in the angrite parent body. *Geochim. Cosmochim. Acta* **212**, 62–83 (2017).

49. K. Righter, K. Nickodem, K. Pando, L. Danielson, A. Boujibar, M. Righter, T. J. Lapen, Distribution of Sb, As, Ge, and In between metal and silicate during accretion and core formation in the Earth. *Geochim. Cosmochim. Acta* **198**, 1–16 (2017).
50. T. A. Suer, J. Siebert, L. Remusat, N. Menguy, G. Fiquet, A sulfur-poor terrestrial core inferred from metal–silicate partitioning experiments. *Earth Planet. Sci. Lett.* **469**, 84–97 (2017).
51. N. R. Bennett, J. M. Brenan, Y. Fei, Thermometry of the magma ocean: Controls on the metal–silicate partitioning of gold. *Geochim. Cosmochim. Acta* **184**, 173–192 (2016).
52. E. Kubik, J. Siebert, I. Blanchard, A. Agranier, B. Mahan, F. Moynier, Earth's volatile accretion as told by Cd, Bi, Sb and Tl core–mantle distribution. *Geochim. Cosmochim. Acta* **306**, 263–280 (2021).
53. D. S. Grewal, N. X. Nie, B. Zhang, A. Izidoro, P. D. Asimow, Accretion of the earliest inner Solar System planetesimals beyond the water snowline. *Nat. Astron.* **8**, 290–297 (2024).
54. H. L. Bercovici, L. T. Elkins-Tanton, J. G. O'rourke, L. Schaefer, The effects of bulk composition on planetesimal core sulfur content and size. *Icarus* **380**, 114976 (2022).
55. A. J. Campbell, M. Humayun, M. K. Weisberg, Siderophile element constraints on the formation of metal in the metal-rich chondrites Bencubbin, Weatherford, and Gujba. *Geochim. Cosmochim. Acta* **66**, 647–660 (2002).
56. A. N. Krot, Y. Amelin, P. Cassen, A. Meibom, Young chondrules in CB chondrites from a giant impact in the early Solar System. *Nature* **436**, 989–992 (2005).
57. M. Weyrauch, J. Zipfel, S. Weyer, Origin of metal from CB chondrites in an impact plume – A combined study of Fe and Ni isotope composition and trace element abundances. *Geochim. Cosmochim. Acta* **246**, 123–137 (2019).
58. P. H. Warren, F. Ulff-Møller, H. Huber, G. W. Kallemeyn, Siderophile geochemistry of ureilites: A record of early stages of planetesimal core formation. *Geochim. Cosmochim. Acta* **70**, 2104–2126 (2006).
59. K. Rankenburg, M. Humayun, A. D. Brandon, J. S. Herrin, Highly siderophile elements in ureilites. *Geochim. Cosmochim. Acta* **72**, 4642–4659 (2008).
60. J. Yang, J. I. Goldstein, J. R. Michael, P. G. Kotula, E. R. D. Scott, Thermal history and origin of the IVB iron meteorites and their parent body. *Geochim. Cosmochim. Acta* **74**, 4493–4506 (2010).
61. H. A. Tornabene, C. D. Hilton, K. R. Bermingham, R. D. Ash, R. J. Walker, Genetics, age and crystallization history of group IIC iron meteorites. *Geochim. Cosmochim. Acta* **288**, 36–50 (2020).
62. C. M. Corrigan, K. Nagashima, C. Hilton, T. J. McCoy, R. D. Ash, H. A. Tornabene, R. J. Walker, W. F. McDonough, D. Rumble, Nickel-rich, volatile depleted iron meteorites: Relationships and formation processes. *Geochim. Cosmochim. Acta* **333**, 1–21 (2022).
63. J. Yang, J. I. Goldstein, E. R. D. Scott, Metallographic cooling rates and origin of IVA iron meteorites. *Geochim. Cosmochim. Acta* **72**, 3043–3061 (2008).
64. J. Yang, J. I. Goldstein, E. R. D. Scott, Iron meteorite evidence for early formation and catastrophic disruption of protoplanets. *Nature* **446**, 888–891 (2007).
65. A. C. Hunt, K. J. Theis, M. Rehkämper, G. K. Benedix, R. Andreasen, M. Schönbächler, The dissipation of the solar nebula constrained by impacts and core cooling in planetesimals. *Nat. Astron.* **6**, 812–818 (2022).
66. M. Matthes, M. Fischer-Gödde, T. S. Kruijer, T. Kleine, Pd-Ag chronometry of IVA iron meteorites and the crystallization and cooling of a protoplanetary core. *Geochim. Cosmochim. Acta* **220**, 82–95 (2018).
67. H. Haack, E. R. D. Scott, S. G. Love, A. J. Brearley, T. J. McCoy, Thermal histories of IVA stony-iron and iron meteorites: Evidence for asteroid fragmentation and reaccretion. *Geochim. Cosmochim. Acta* **60**, 3103–3113 (1996).
68. A. Ruzicka, M. Hutson, Differentiation and evolution of the IVA meteorite parent body: Clues from pyroxene geochemistry in the Steinbach stony-iron meteorite. *Meteorit. Planet. Sci.* **41**, 1959–1987 (2006).
69. E. S. Steenstra, C. J. Renggli, J. Berndt, S. Klemme, Evaporation of moderately volatile elements from metal and sulfide melts: Implications for volatile element abundances in magmatic iron meteorites. *Earth Planet. Sci. Lett.* **622**, 118406 (2023).
70. M. Weyrauch, J. Zipfel, S. Weyer, The relationship of CH, CB, and CR chondrites: Constraints from trace elements and Fe-Ni isotope systematics in metal. *Geochim. Cosmochim. Acta* **308**, 291–309 (2021).
71. D. S. Grewal, P. D. Asimow, Origin of the superchondritic carbon/nitrogen ratio of the bulk silicate Earth – An outlook from iron meteorites. *Geochim. Cosmochim. Acta* **344**, 146–159 (2023).
72. C. M. O. D. Alexander, M. Fogel, H. Yabuta, G. D. Cody, The origin and evolution of chondrites recorded in the elemental and isotopic compositions of their macromolecular organic matter. *Geochim. Cosmochim. Acta* **71**, 4380–4403 (2007).
73. M. Matthes, J. A. van Orman, T. Kleine, Closure temperature of the Pd-Ag system and the crystallization and cooling history of IIIAB iron meteorites. *Geochim. Cosmochim. Acta* **285**, 193–206 (2020).
74. B. Luais, Isotopic fractionation of germanium in iron meteorites: Significance for nebular condensation, core formation and impact processes. *Earth Planet. Sci. Lett.* **262**, 21–36 (2007).
75. E. Wölfer, C. Burkhardt, T. Kleine, "Investigating planetary volatile depletion processes by germanium isotopes in magmatic iron meteorites," in *55th Lunar and Planetary Science Conference* (2024), p. 3040.
76. M. C. Bishop, F. Moynier, C. Weinstein, J. G. Fraboulet, K. Wang, J. Foriel, The Cu isotopic composition of iron meteorites. *Meteorit. Planet. Sci.* **47**, 268–276 (2012).
77. H. Chen, B. M. Nguyen, F. Moynier, Zinc isotopic composition of iron meteorites: Absence of isotopic anomalies and origin of the volatile element depletion. *Meteorit. Planet. Sci.* **48**, 2441–2450 (2013).
78. M. A. Antonelli, S.-T. Kim, M. Peters, J. Labidi, P. Cartigny, R. J. Walker, J. R. Lyons, J. Hoek, J. Farquhar, Early inner solar system origin for anomalous sulfur isotopes in differentiated protoplanets. *Proc. Natl. Acad. Sci. U.S.A.* **111**, 17749–17754 (2014).
79. E. D. Young, A. Shahar, F. Nimmo, H. E. Schlichting, E. A. Schauble, H. Tang, J. Labidi, Near-equilibrium isotope fractionation during planetesimal evaporation. *Icarus* **323**, 1–15 (2019).
80. F. M. Richter, Timescales determining the degree of kinetic isotope fractionation by evaporation and condensation. *Geochim. Cosmochim. Acta* **68**, 4971–4992 (2004).
81. Z. Zhang, D. Bercovici, Generation of a measurable magnetic field in a metal asteroid with a rubble-pile core. *Proc. Natl. Acad. Sci. U.S.A.* **120**, e2221696120 (2023).
82. J. Yang, J. I. Goldstein, Metallographic cooling rates of the IIIAB iron meteorites. *Geochim. Cosmochim. Acta* **70**, 3197–3215 (2006).
83. D. S. Grewal, R. Dasgupta, B. Marty, A very early origin of isotopically distinct nitrogen in inner Solar System protoplanets. *Nat. Astron.* **5**, 356–364 (2021).
84. D. S. Grewal, Origin of nitrogen isotopic variations in the rocky bodies of the solar system. *Astrophys. J.* **937**, 123 (2022).
85. D. S. Grewal, S. Bhattacharjee, G.-D. Mardaru, P. D. Asimow, Tracing the origin of volatiles on Earth using nitrogen isotope ratios in iron meteorites. *Geochim. Cosmochim. Acta* **388**, 34–47 (2025).
86. C. Sturtz, A. Limare, M. Chaussidon, É. Kaminski, Structure of differentiated planetesimals: A chondritic fridge on top of a magma ocean. *Icarus* **385**, 115100 (2022).
87. E. Kaminski, A. Limare, B. Kenda, M. Chaussidon, Early accretion of planetesimals unraveled by the thermal evolution of the parent bodies of magmatic iron meteorites. *Earth Planet. Sci. Lett.* **548**, 116469 (2020).
88. T. Lichtenberg, G. J. Golabek, T. V. Gerya, M. R. Meyer, The effects of short-lived radionuclides and porosity on the early thermo-mechanical evolution of planetesimals. *Icarus* **274**, 350–365 (2016).
89. A. Gargano, Z. Sharp, The chlorine isotope composition of iron meteorites: Evidence for the Cl isotope composition of the solar nebula and implications for extensive devolatilization during planet formation. *Meteorit. Planet. Sci.* **54**, 1619–1631 (2019).
90. G. D. Bromiley, The geochemical legacy of low-temperature, percolation-driven core formation in planetesimals. *Earth Moon Planets* **127**, 4 (2023).
91. M. Collinet, T. L. Grove, Incremental melting in the ureilite parent body: Initial composition, melting temperatures, and melt compositions. *Meteorit. Planet. Sci.* **55**, 832–856 (2020).
92. A. Ruzicka, Silicate-bearing iron meteorites and their implications for the evolution of asteroidal parent bodies. *Geochemistry* **74**, 3–48 (2014).
93. T. Kleine, T. Steller, C. Burkhardt, F. Nimmo, An inner solar system origin of volatile elements in Mars. *Icarus* **397**, 115519 (2023).
94. R. Martins, S. Kuthning, B. J. Coles, K. Kreissig, M. Rehkämper, Nucleosynthetic isotope anomalies of zinc in meteorites constrain the origin of Earth's volatiles. *Science* **379**, 369–372 (2023).
95. T. Steller, C. Burkhardt, C. Yang, T. Kleine, Nucleosynthetic zinc isotope anomalies reveal a dual origin of terrestrial volatiles. *Icarus* **386**, 115171 (2022).
96. P. S. Savage, F. Moynier, M. Boyet, Zinc isotope anomalies in primitive meteorites identify the outer solar system as an important source of Earth's volatile inventory. *Icarus* **386**, 115172 (2022).
97. N. X. Nie, D. Wang, Z. A. Torrano, R. W. Carlson, C. M. O' D Alexander, A. Shahar, Meteorites have inherited nucleosynthetic anomalies of potassium-40 produced in supernovae. *Science* **379**, 372–376 (2023).
98. M. Paquet, P. A. Sossi, F. Moynier, Origin and abundances of volatiles on Mars from the zinc isotopic composition of Martian meteorites. *Earth Planet. Sci. Lett.* **611**, 118126 (2023).
99. N. Dauphas, A. Pourmand, Hf–W–Th evidence for rapid growth of Mars and its status as a planetary embryo. *Nature* **473**, 489–492 (2011).
100. N. Braukmüller, F. Wombacher, C. Funk, C. Münker, Earth's volatile element depletion pattern inherited from a carbonaceous chondrite-like source. *Nat. Geosci.* **12**, 564–568 (2019).
101. B. Bourdon, M. Roskosz, R. C. Hin, Isotope tracers of core formation. *Earth Sci. Rev.* **181**, 61–81 (2018).
102. D. R. Haughton, P. L. Roeder, B. J. Skinner, Solubility of sulfur in mafic magmas. *Econ. Geol.* **69**, 451–467 (1974).
103. Z. Ma, Thermodynamic description for concentrated metallic solutions using interaction parameters. *Metall. Mater. Trans. B* **32**, 87–103 (2001).
104. K. Zhu, F. Moynier, D. Wielandt, K. K. Larsen, J.-A. Barrat, M. Bizzarro, Timing and origin of the angrite parent body inferred from Cr isotopes. *Astrophys. J. Lett.* **877**, L13 (2019).

105. J. F. J. Bryson, J. A. Neufeld, F. Nimmo, Constraints on asteroid magnetic field evolution and the radii of meteorite parent bodies from thermal modelling. *Earth Planet. Sci. Lett.* **521**, 68–78 (2019).
106. E. S. Steenstra, J. S. Knibbe, N. Rai, W. van Westrenen, Constraints on core formation in Vesta from metal–silicate partitioning of siderophile elements. *Geochim. Cosmochim. Acta* **177**, 48–61 (2016).
107. G. J. Taylor, Core formation in asteroids. *J. Geophys. Res.* **97**, 14717–14726 (1992).
108. A. J. G. Jurewicz, D. W. Mittlefehldt, J. H. Jones, Experimental partial melting of the St. Severin (LL) and Lost City (H) chondrites. *Geochim. Cosmochim. Acta* **59**, 391–408 (1995).
109. A. J. G. Jurewicz, D. W. Mittlefehldt, J. H. Jones, Experimental partial melting of the Allende (CV) and Murchison (CM) chondrites and the origin of asteroidal basalts. *Geochim. Cosmochim. Acta* **57**, 2123–2139 (1993).
110. J. T. Wasson, G. W. Kallemeyn, Compositions of chondrites. *Phil. Trans. R. Soc. A Math. Phys. Eng. Sci.* **325**, 535–544 (1988).
111. N. L. Chabot, E. A. Wollack, W. F. McDonough, R. D. Ash, S. A. Saslow, Experimental determination of partitioning in the Fe-Ni system for applications to modeling meteoritic metals. *Meteorit. Planet. Sci.* **52**, 1133–1145 (2017).
112. J. H. Jones, D. J. Malvin, A nonmetal interaction model for the segregation of trace metals during solidification of Fe-Ni-S, Fe-Ni-P, and Fe-Ni-S-P alloys. *Metall. Trans. B* **21**, 697–706 (1990).
113. J. T. Wasson, Trapped melt in IIIAB irons; solid/liquid elemental partitioning during the fractionation of the IIIAB magma. *Geochim. Cosmochim. Acta* **63**, 2875–2889 (1999).
114. B. J. Wood, D. J. Smythe, T. Harrison, The condensation temperatures of the elements: A reappraisal. *Am. Min.* **104**, 844–856 (2019).
115. C. M. O. Alexander, Quantitative models for the elemental and isotopic fractionations in chondrites: The carbonaceous chondrites. *Geochim. Cosmochim. Acta* **254**, 277–309 (2019).
116. T. Yoshizaki, W. F. McDonough, The composition of Mars. *Geochim. Cosmochim. Acta* **273**, 137–162 (2020).
117. H. S. Wang, C. H. Lineweaver, T. R. Ireland, The elemental abundances (with uncertainties) of the most Earth-like planet. *Icarus* **299**, 460–474 (2018).

Acknowledgments: We thank A. P. Vyas for helping to improve the clarity of communication. **Funding:** This study was supported by startup funds from ASU to D.S.G. **Author contributions:** D.S.G. conceived the project and compiled the data. D.S.G. performed the numerical calculations with S.B. and B.Z. All authors interpreted the data. D.S.G. wrote the manuscript with inputs from all authors. **Competing interests:** The authors declare that they have no competing interests. **Data and materials availability:** All data needed to evaluate the conclusions in the paper are present in the paper and/or the Supplementary Materials.

Submitted 5 June 2024
Accepted 3 January 2025
Published 5 February 2025
10.1126/sciadv.adq7848